Journal of Manufacturing Processes 147 (2025) 177–190

Contents lists available at ScienceDirect

Journal of Manufacturing Processes

journal homepage: www.elsevier.com/locate/manpro

Relationship between associated acoustic emission and crack position during directed energy deposition of a metal matrix composite

Md Jonaet Ansari [a,b,*], Anthony Roccisano [a,b], Elias J.G. Arcondoulis [c], Christiane Schulz [a,d], Thomas Schläfer [d], Colin Hall [a,b]

[a] Future Industries Institute, University of South Australia, Mawson Lakes, SA 5095, Australia
[b] The Australian Research Council (ARC) Industrial Transformation Training Centre in Surface Engineering for Advanced Materials (SEAM), University of South Australia, Mawson Lakes, SA 5095, Australia
[c] School of Civil Aerospace and Design Engineering, University of Bristol, Bristol, UK
[d] LaserBond Ltd, Cavan, SA 5094, Australia

ARTICLE INFO

Keywords:
Acoustic emission
Crack detection
Directed energy deposition

ABSTRACT

Laser-based directed energy deposition (DED) is a versatile additive manufacturing (AM) technique capable of depositing high-quality coatings, repairing components, and fabricating complex metal matrix composite structures. The DED process, however, is prone to defects, particularly cracking, due to dynamic thermal gradients and residual stresses inherent in the process. Conventional monitoring methods, such as optical and thermal imaging, primarily focus on surface defects and often fail to detect subsurface cracks, that can significantly affect the structural integrity of fabricated structures. This study presents a novel acoustic emission (AE)-based monitoring method capable of detecting and quantifying both surface and subsurface cracks during the DED process. By exploiting the exponential decay of the unique acoustic emissions due to DED, the second-order derivative of the acoustic signal is invariant, thereby filtering extraneous noise sources and hence yielding a robust methodology for relating DED-based cracking initiation times and their associated positions. The results reveal that crack formation timing and location vary significantly with energy density. The novel techniques were used to show that higher energy density leads to slower cooling and solidification rates, resulting in delayed crack formation and detection further behind the laser beam's position.

1. Introduction

Laser-based directed energy deposition (DED) is one of the leading metal AM techniques used industrially. This advanced process employs a focused laser beam to selectively melt and deposit metallic materials, usually in powder or wire form, onto a substrate. The feedstock material is precisely introduced into the laser-generated melt pool, enabling the accurate layer-by-layer addition of new material [1,2]. DED offers significant advantages for manufacturing large-scale parts and complex geometries due to its high deposition rates. Its ability to repair high-value components and apply wear and corrosion resistance coatings further enhances its practicality and adoption in industries. The versatility, efficiency, and compatibility with a wide range of metals and alloys contribute to DED's prominence in aerospace, automotive, and heavy industries [3–6].

While the DED process has numerous advantages, it encounters considerable difficulties in maintaining uniform part quality and ensuring process reliability. These issues are primarily attributed to its high sensitivity to multiple process variables, such as laser power, scanning speed, and powder feed rate [7–9]. Such sensitivity necessitates manufacturers to extensively explore and optimize a vast array of material compositions and process variables before proceeding to final production. The optimization process, whether conducted through trial-and-error methods or advanced machine learning techniques, is often resource-intensive and time-consuming. Moreover, even with the best-optimized parameters, the inherent thermal variability and complexity of the melt pool dynamics can still initiate process-induced defects such as cracks and porosity.

In DED-fabricated structures, cracks are the most typical defects, primarily attributed to the intricate thermal dynamics and resulting residual stress accumulation inherent to the process [10,11]. The DED technique involves a complex thermal field characterized by abrupt

* Corresponding author at: Future Industries Institute, University of South Australia, Mawson Lakes, SA 5095, Australia.
E-mail address: md_jonaet.ansari@mymail.unisa.edu.au (M.J. Ansari).

https://doi.org/10.1016/j.jmapro.2025.05.015
Received 22 October 2024; Received in revised form 22 April 2025; Accepted 13 May 2025
Available online 19 May 2025

temperature fluctuations, which generate significant temperature gradients within the material. These gradients lead to thermal expansion and contraction, generating residual stresses within the material. As the deposited layers cool and solidify, the accumulated stresses can exceed the material's tensile strength, resulting in crack formation [12,13]. As the process continues, the interaction between the melt pool and pre-existing cracks can exacerbate the issue. The repeated thermal cycling during layer deposition contributes to the accumulation of high residual stresses. These stresses can not only cause the formation of new cracks but also lead to the reopening and propagation of existing ones. When the accumulated stresses exceed the material's tensile strength, crack reformation and growth occur within the deposited layers [14,15]. This cyclical process of stress accumulation and crack propagation poses a significant challenge in maintaining the structural integrity of DED-fabricated structures. Non-destructive testing (NDT) methods, such as dye penetrant inspection, ultrasonic testing, radiographic testing, and eddy current testing, are commonly employed by manufacturers to detect defects in fabricated structures [16]. However, these traditional post-manufacturing techniques have significant limitations in AM processes like DED and powder bed fusion (PBF). Firstly, they are limited to being performed after production is completed, preventing in-situ defect detection and correction throughout the fabrication process. Secondly, while some methods like ultrasonic and radiographic testing can detect subsurface flaws, others like dye penetrant inspection are limited to surface defect detection, potentially missing internal defects that could compromise the integrity of the part.

Given these limitations, there is an urgent requirement for in-situ defect detection techniques capable of providing insights into the layer-by-layer formation of cracks during DED processing. This capability significantly reduces the time and cost of post-process quality inspection and qualification tasks for fabricated structures. Manufacturers can quickly assess part quality by identifying defects as they form without relying solely on time-consuming and expensive post-production inspections. Additionally, real-time defect detection opens possibilities for corrective actions. While it may not always be feasible to prevent cracks once they've initiated, early detection allows for immediate process adjustments that could limit defect propagation or severity. Recent advancements in in-situ process monitoring techniques have significantly enhanced our ability to capture and analyse critical process signatures during the DED process. Vision-based systems, thermal sensors, acoustic emission (AE) sensing, and X-ray imaging have emerged as powerful tools for observing melt pool behaviour, tracking thermal profiles, and detecting acoustic signatures resulting from laser-material interactions [17–19]. These sophisticated monitoring methods provide real-time insights into the complex phenomena occurring during fabrication. Furthermore, the integration of artificial intelligence (AI) technology with these monitoring techniques has revolutionized real-time defect detection capabilities [20,21]. AI algorithms can rapidly process and interpret the vast amounts of data generated by these sensors, enabling more accurate and efficient identification of potential defects during the fabrication process.

Vision-based process monitoring methods, when coupled with advanced data analysis techniques, have significantly enhanced the ability to extract geometric features from melt pool images, which are crucial for quality inspection and defect detection in DED process [22–27]. Infrared (IR) thermal imaging systems offer significant benefits by capturing temperature-related features of the melt pool, often providing more comprehensive information than vision-based systems alone [22–25]. Machine learning (ML) algorithms are essential for analysing these captured temperature-related features. These algorithms enable the identification of subtle variations in temperature distribution, thermal gradients, and cooling rates, which are crucial indicators of process stability and potential defect formation [28–30]. However, vision- and thermal-based monitoring methods are limited in their ability to provide detailed information about sub-surface crack initiation and propagation phenomena. Specifically, these methods do not adequately capture the interaction between the melt pool and pre-existing cracks, the mechanisms of crack reformation, or the precise locations of crack formation relative to the laser beam. This gap underscores the importance of developing more advanced monitoring techniques to fully understand and mitigate crack formation during the DED process.

To address these limitations, advanced X-ray imaging techniques offer valuable insights into laser-material interactions and defect formation mechanisms during AM process [31–34]. This advanced imaging technique allows for the real-time observation of crack initiation and propagation phenomena, offering valuable information on how and where cracks form and spread within the deposited structures [35].

In PBF processes with low energy density (7.27 W/mm^2), cracks appeared and grew towards the top surface with delays of 2.7–4.4 ms after laser-material interaction [36]. In DED processes with high energy density (125 W/mm^2), crack growth was observed approximately 500 ms after the laser beam traversed pre-existing cracks [37]. This observation demonstrates a trend of decreasing time for crack development and propagation to the surface as residual stresses accumulate. These findings highlight the dynamic nature of crack growth in DED-fabricated structures, revealing the complex interplay between thermal cycling and residual stress accumulation. From the above information, there is a delay between the laser-material interaction phenomenon and the occurrence, remelting, and propagation of cracks along the building direction. However, camera-based techniques primarily focus on the melt pool and its adjacent regions. Given the observed delay between laser-material interaction and crack occurrence or propagation, these methods may not capture the full dynamics of crack formation phenomena. This limitation underscores the need for additional monitoring techniques that can detect sub-surface defects or delayed crack formation.

Acoustic emission (AE) monitoring presents a promising solution to address the limitations of camera-based techniques in identifying both surface and sub-surface defects during DED process [38]. This technique captures and analyses acoustic signatures emitted during laser-material interaction and material fracture, providing valuable insights into the process-induced defects formation. The real-time, continuous monitoring capabilities of AE throughout the build process allow for the detection of defects as they form, including delayed crack formation that may occur after the initial laser-material interaction [39]. Acoustic sensors designed to detect structure-borne sounds can capture signals generated by crack propagation and other defects within workpieces during the DED process. For instance, Taheri et al. [40] developed a specialized structure-borne sensor affixed to the substrate of the part being built to capture acoustic emissions. Their research demonstrated that acoustic signals of the DED process could be categorized to distinguish manufacturing conditions and quantitatively analyse cluster cohesion and isolation. Using a K-Mean clustering algorithm, they established a connection between acoustic signatures and fabricated part quality, achieving classification accuracies exceeding 87 % for most process conditions. Kaiqiang et al. [41] demonstrated the effectiveness of AE detection for monitoring both deposition state and crack defect activity during the DED process. The study developed two specialized neural networks: one for deposition state recognition and another for crack detection. By classifying AE signals into low-energy and high-energy categories, the method accurately identified the impacts of numerous DED parameters on the deposition state and detected crack defects caused by abnormal process conditions. Crack-related AE signals were observed to be up to 100 times higher in amplitude than base deposition state signals, potentially masking underlying state information. However, structure-borne sensors have significant limitations in DED applications. The high temperatures inherent to the DED process can potentially damage these sensors when attached directly to workpieces, and their fixed positioning lacks the flexibility offered by airborne acoustic sensors, which can be placed at a safe distance from the processing zone. Airborne acoustic sensors, such as condenser and

optical microphones, have been employed in numerous studies to capture acoustic signatures during DED processing. García de la Yedra et al. [42] utilized an optical microphone to capture airborne acoustic waves for detecting layer cracks in DED process. Their research revealed distinct peak values in the acoustic signals with notably high amplitudes, clearly indicating material fracture and energy release attributed to both initial cracking and subsequent crack growth. This phenomenon is fundamentally linked to the nature of cracking as an energy-releasing process, wherein the abrupt release of stored elastic energy during crack propagation generates distinctive acoustic waves. The unique patterns observed in the AE signals reflected the sudden rise in acoustic energy generated by crack formation and growth. Kim et al. [43] utilized condenser microphone to capture audible cracks occurred during the DED process. Specifically, their research reveals that micro-cracking generates a distinctive acoustic signature within a frequency range of 12,000 to 16,000 Hz.

However, in industrial settings, the airborne sounds generated during the DED operation are characterized by a complex interplay of defect-related events and various disturbances. These disturbances encompass a wide range of sources, including mechanical noise generated by the robotic laser head's movement, audible flows of carrier and shielding gases, human interactions near the process area, and ambient noise from surrounding machinery. To address these challenges, recent advancements in signal processing techniques for acoustic monitoring in DED have integrated ML approaches, focusing on extracting meaningful acoustic features from raw signals, encompassing time-domain, frequency-domain, and wavelet-based characteristics [44–48]. The primary challenge in this field lies in establishing robust correlations between these extracted acoustic features and location-specific defects that occur during the DED process. Advanced ML algorithms are being developed to identify relevant acoustic signatures while effectively filtering out extraneous noise, thereby facilitating a more precise focus on defect-indicative patterns.

For instance, Chen et al. [49] introduced an innovative deep learning-based framework for signal denoising in acoustic monitoring of the DED process. The framework integrated audio equalization, bandpass filtering, and Harmonic-Percussive Source Separation (HPSS) algorithms, creating a synergistic method capable of significantly reducing background noise and isolating laser-material interaction acoustic signals. By leveraging the power of deep learning, the framework demonstrated remarkable efficacy in extracting clean, meaningful acoustic data from raw, noise-contaminated signals. In subsequent research, Chen et al. [50] further advanced their approach by extracting Mel-frequency Cepstrum Coefficients (MFCCs) as acoustic features from the denoised signals. These features were then utilized for training a convolutional neural network (CNN) to predict crack formation, keyhole pore occurrence, and defect-free regions. The CNN architecture, when trained on denoised dataset, established excellent performance compared to other models, achieving the highest overall accuracy of 89 % and a keyhole pore prediction accuracy of 93 %. Building upon these findings, a more comprehensive multi-sensor fusion-based digital twin (MFDT) in-situ process monitoring system was developed. This advanced system integrated multiple data sources, including visual, thermal, and acoustic data captured during the DED process, and employed multiple supervised ML algorithms to predict location-specific defect occurrences in fabricated structures. The MFDT system significantly outperformed conventional single-sensor defect detection techniques, achieving a higher overall accuracy of 96 % and a reduced false alarm rate of 4.4 % [51]. However, the primary limitation of this study was its focus on predicting defective regions rather than identifying individual defects. Instead of identifying specific cracks or keyhole pores, the method predicted entire 500 ms intervals (corresponding to approx. 12 mm sections) as defective if any defect was present within that region. This approach effectively identified problematic areas but lacked precision in differentiating defect types or pinpointing their exact locations, potentially leading to over-classification of defective regions.

In our previous study, we introduced an AE technique specifically optimized for identifying audible crack events that occur during industrial DED operations. Our developed signal processing algorithm effectively identified genuine acoustic events associated with crack formation, successfully distinguishing them from external disturbances. This method demonstrated robust performance in the complex, noise-rich environments typical of industrial settings, enhancing the reliability of crack detection in challenging manufacturing conditions.

This study advances the application of a previously established signal processing technique for AE analysis, specifically addressing critical challenges in understanding crack formation during the DED process. The work's novelty lies in its comprehensive approach to both surface and sub-surface regions, employing a layer-by-layer examination of acoustic signals throughout the DED process. By providing deeper insights into crack initiation and propagation between deposited layers, this method bridges existing knowledge gaps in the field. The technique correlates acoustic events with spatial and temporal data, enabling the tracking of potential crack locations and growth over time. Through analysis of acoustic signatures across successive layers, the study explains mechanisms of crack reformation and precisely locates crack formation relative to the laser beam position. This approach facilitates a comprehensive understanding of crack initiation, propagation, and reformation mechanisms throughout the buildup process, contributing to the development of more effective defect mitigation strategies in DED process.

2. Experimental methods

The research employed an industrial DED system integrating four near-infrared diode lasers, with a collective output of up to 16 kW. The laser beam featured a top-hat profile, ensuring uniform energy distribution across its diameter. A commercially available nickel-based metal matrix composite (MMC) powder was selected as the feedstock material due to its widespread use in aerospace, automotive, and energy sectors. Although the material has a robust process window under optimized conditions, it is also known to exhibit cracking sensitivity during DED processing when operated outside of this window, including instances of single-track deposition. The deposition was carried out on a flat mild steel substrate. The fabrication process involved the production of two thin-wall structures, each built as a single track with 6 layers, deposited using a unidirectional laser scanning pattern. An inter-layer idle time of 7.1 s was implemented to allow for adequate cooling and stabilization between successive layers. The process parameters, presented in Table 1, were specifically selected to favor crack formation. To investigate acoustic waves generated from delayed crack formation, the energy density was systematically varied across experiments. The experimental setup for real-time capturing of airborne acoustic waves emitted during the DED process is illustrated in Fig. 1.

An advanced AE monitoring system was utilized to capture real-time acoustic waves emitted from the laser-material interactions and crack formation events. The system comprised a 1/4 in. omnidirectional free-field microphone (MPA416, BSWA Technology Co., Ltd.) integrated with a National Instruments (NI) Data Acquisition (DAQ) setup, consisting of an NI-9234C Series Sound and Vibration Input Module and a cDAQ-9174 CompactDAQ chassis [52]. The microphone was positioned 1 m from the deposition zone and 0.3 m above the substrate surface, as illustrated in Fig. 1. This placement was chosen to allow for capturing a broader range of acoustic signals emitted during the fabrication process, including those associated with defects such as crack. The microphone recorded acoustic signals within a frequency range of 20 to 20 kHz, and the data was acquired at a sampling rate of 51.2 kHz, allowing for high-resolution capture of the acoustic signals. A custom-developed MATLAB program interfaced with the DAQ system facilitated in-situ collection and storage of acoustic data throughout the fabrication process. Following this, the acquired acoustic data was thoroughly analyzed through a sequence of signal processing techniques executed via a

Table 1
Process parameters utilized for the DED experiments.

Track	Laser power, P (W)	Laser spot diameter, d (mm)	Scanning speed, v mm/min	Energy density, $E = P / (v \times d)$ W/mm^2	Total deposition time, t s	Deposited track length. L mm
#1	4000	4.8	1000	50	7.905	132
#2	4500	4.8	800	70	9	120

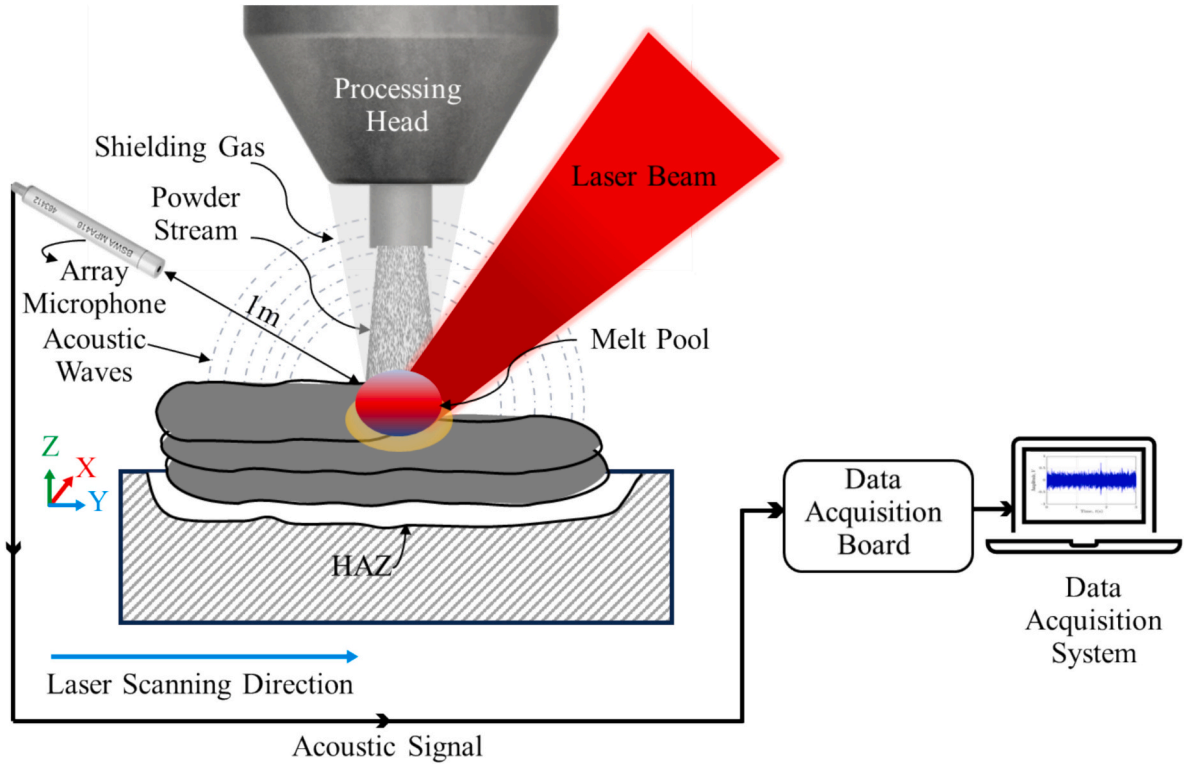

Fig. 1. Schematic representation of the experimental setup for real-time acoustic emission monitoring during the DED process, adapted from [52].

customized MATLAB program.

Upon completing the DED process, the deposited tracks were air cooled to room temperature. Following this, the tracks were longitudinally sectioned utilizing wire electrical discharge machining, as shown in Fig. 2. The sectioned samples were then subjected to metallographic preparation. Initially, the samples were mechanically ground followed by a multi-stage polishing regimen employing diamond suspensions of progressively smaller particle sizes. For comprehensive microstructural examination, the prepared samples were analyzed using an Olympus DSX1000 Digital Microscope. This microscope was utilized to take high-resolution pictures of the longitudinally sectioned specimens, enabling detailed visualization of the any process-induced defects located inside

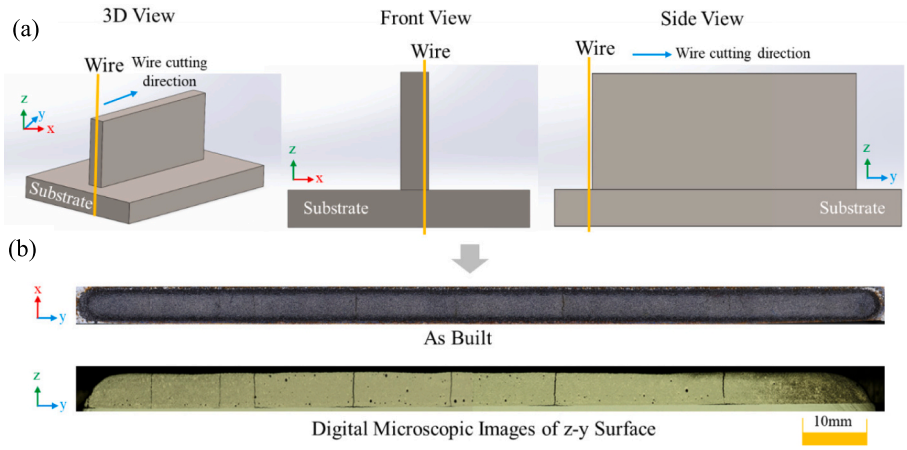

Fig. 2. Illustration of the sample preparation process: (a) Longitudinal wire-cutting schematic for sectioning DED-fabricated samples, (b) Digital microscopic imaging of the as-built and prepared sample (laser scanning direction is from left to right).

the fabricated track.

3. Crack detection method

The analysis of airborne acoustic signals recorded during the DED process was conducted using previously developed signal-processing techniques [52]. This established methodology, detailed in our earlier work, was specifically designed to detect crack events, and distinguish them from random background noise. The raw time-series signals recorded during and after the single-track deposition process are illustrated in Fig. 3. To enhance visualization, the raw signals were color-coded to represent different phases of the DED process: blue sections corresponded to active laser deposition, while red sections indicated periods of laser inactivity. Upon closer examination, it became evident that the raw signals contained a complex mixture of cracks, normal process emissions (non-cracks), and various disturbance events such as mechanical noise generated by the robotic laser head's movement, audible flows of carrier and shielding gases, human interactions near the process area, and ambient noise from surrounding machinery. This complexity in the raw signals presented a significant challenge in distinguishing crack-related emissions from other acoustic events based solely on time-domain analysis. The normal process emissions represent continuous, low-amplitude signals occurring during crack-free operation, while disturbance events are characterized by high-amplitude, longer-duration acoustic signatures resulting from external factors unrelated to the DED process. Moreover, this detailed analysis revealed that both crack and disturbance events appear as burst signals with high-amplitude features, as illustrated in Fig. 3(b) and Fig. 3(c), thus complicating their distinction in the time domain.

To gain additional insights, Fig. 3(d) presents the time-frequency representations of these raw acoustic signals achieved through Short-Time Fourier Transform (STFT). This analysis demonstrates that both crack events and various disturbances (previously described) exhibit prominence in overlapping frequency ranges (4–18 kHz for cracks, 8–18 kHz for disturbances). Consequently, the overlapping frequency ranges make it challenging to reliably distinguish between crack and disturbance events using only time-frequency features. The limitations of time and frequency domain analyses necessitate the development of more sophisticated signal processing techniques to accurately identify and characterize crack events within the complex acoustic signals generated during the DED process. To address this challenge, our study introduced

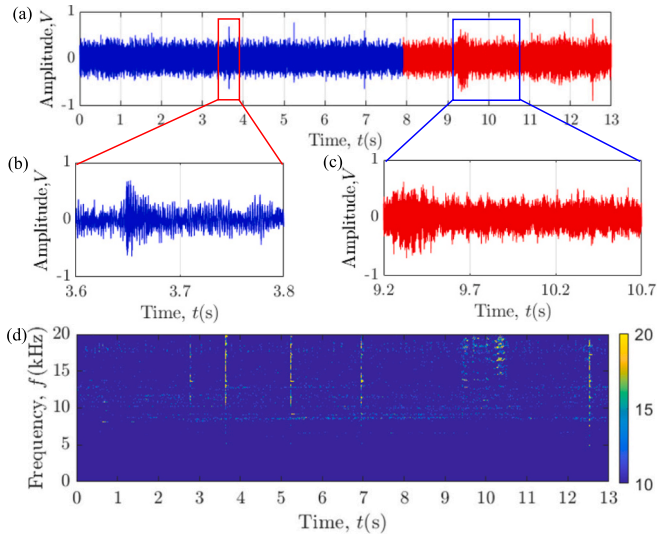

Fig. 3. Analysis of acoustic signals for crack detection during the DED process, (a) raw time-series signals containing a mixture of crack events and disturbances, (b) raw acoustic signals of a crack, (c) raw acoustic signal of disturbance, and (d) the time-frequency representations of these raw acoustic signals.

a novel signal processing approach based on the observation that acoustic waves emitted from cracks follow an exponential amplitude decay pattern, whereas disturbance events lack this characteristic due to their distinct origins or mechanisms. Crack events with exponential decay signatures were retained when computing the second-order derivatives of raw time-series signals, whereas disturbances that do not exhibit exponential decay were completely suppressed.

For instance, a crack event occurred between 3 s and 4 s, and some disturbance events occurred between 9 s and 11 s in the raw time-series signals, as illustrated in Fig. 4(a). However, in the processed signal (Fig. 4(b)), during the same time frame, the disturbance events were completely attenuated, while the acoustic signatures of crack events were enhanced relative to those derived from the raw acoustic signals. This is evident in Fig. 4(c), where a sudden amplitude change occurred at the initiation of the cracks, followed by an exponential decrease from the peak amplitudes. In some cases, the acoustic signals of certain disturbance events remain prominent even after applying second-order derivatives calculations, particularly the events illustrated in Fig. 4(d), located from 10.2 s to 10.7 s in the processed signal. In such cases, the developed method differentiates between crack events and disturbances based on their exponential amplitude decay behaviour. The system utilizes a variable threshold crossing method to detect sudden amplitude fluctuations that mark the initiation of potential crack or disturbance events. Following the identification of these change points, it establishes processing windows between each pair and locates the highest peaks within each window, as shown in Fig. 4(e). To examine the exponential amplitude decay pattern identified in the acoustic signals of crack events, the algorithm fits an exponential decay function ($y = y0 + ae^{-x/c}$) to the normalized acoustic signals. The constant, c in the exponential decay function indicates how rapidly the signals amplitude decreases after the peak. The examination revealed that crack events (crack 1 & 2) generated an c-values of 5.0 and 8.4 whereas the disturbance event had a significantly higher c-value of 44, as presented in Fig. 4(f). A histogram of c-values, derived from an extensive analysis of 678 events (497 cracks and 181 disturbances), is presented in Fig. 4(g). Statistical examination of these results established that c-values between 4 and 21 are indicative of crack events. Acoustic signals yielding c-values beyond this range are consequently classified as non-cracking or disturbance events. The clear separation of c-values between crack events (4–21) and disturbances (>21), as exemplified by the provided examples (5.0 and 8.4 for crack events versus 44 for disturbances), demonstrates the method's effectiveness in identifying crack events, as illustrated in Fig. 4(h). This developed signal processing technique was then utilized to analyse all the captured acoustic signals generated during multilayered DED experiments, enabling more accurate detection and characterization of crack formation in real-time. The results of this analysis are presented in the following sections, showcasing the method's capacity to distinguish crack events from external disturbances in the complex acoustic environment of the DED process.

4. Results & discussion

4.1. Layer-by-layer crack detection

The acoustic signals recorded throughout the single-track multi-layered DED process under both low and high energy density settings were analyzed using the newly developed signal processing technique. The results obtained under low energy density conditions are presented in Fig. 5.

The comprehensive results of the acoustic analysis across all layers, displaying identified crack events and their occurrence times throughout the entire build process are presented in Fig. 5. In Fig. 5(a), the processed signal was color-coded to represent different phases of the DED process: blue sections correspond to active laser deposition, while red sections indicate periods when the laser was off (no deposition). The start of the blue section (laser on) and the end of the blue section (laser

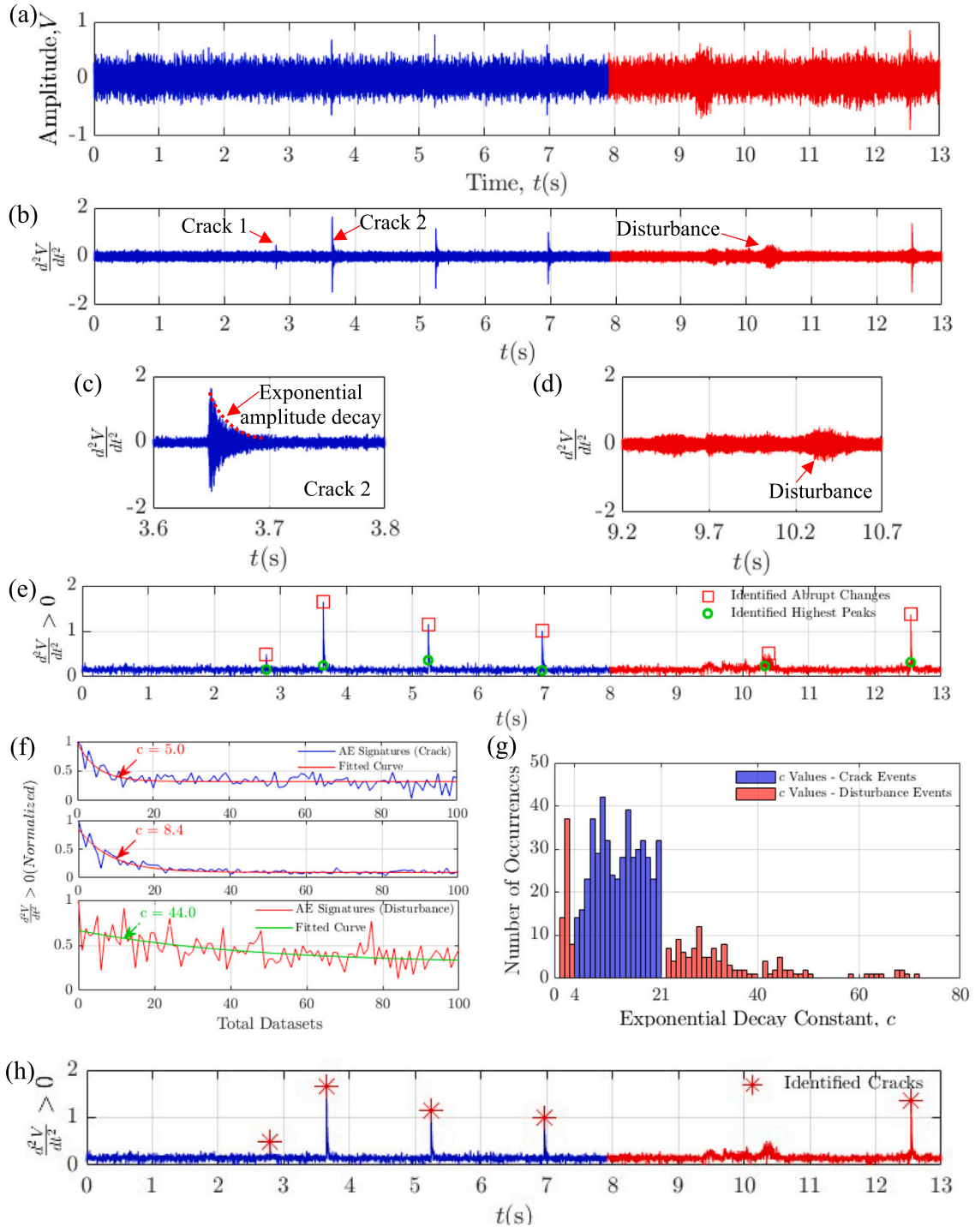

Fig. 4. (a) Raw time-series signals containing a mixture of crack events and disturbances, (b) second-order derivatives of raw signals, (c) processed acoustic signatures of crack 2, (d) processed acoustic signatures of disturbances, (e) detected sudden amplitude variations (red squares) and peak values (light green dots) in the processed signals, (f) Exponential decay function fitting for cracks (crack 1 and crack 2) and disturbances, (g) histogram of c-values, (h) identified crack events in the processed signals. (For interpretation of the references to color in this figure legend, the reader is referred to the web version of this article.)

off) specify the beginning and ending of the deposition process. This color-coded representation effectively defines the initiation and conclusion of the deposition process for each individual layer, providing a clear temporal structure to the acoustic data. The developed signal processing method successfully identified actual crack events that occurred in different layers and distinguished them from non-cracking/disturbance events. This differentiation is based on the unique acoustic signatures associated with crack formation, characterized by an exponential decay constant (c-value) within a specific range established through statistical analysis of numerous events.

The layer-by-layer analysis of the processed acoustic signals, illustrating the distribution and occurrence of crack events across individual layers of the DED process, is shown in Fig. 5(b). It also presented to describe the sub-surface crack growth and propagation phenomenon based on the timing of crack occurrences within each layer. The timeline of the analysis spans from $t = 0$ s, representing the start of deposition, to $t = 13$ s, extending beyond the completion of the deposition process at $t = 7.9$ s. This extended timeframe was deliberately chosen to capture

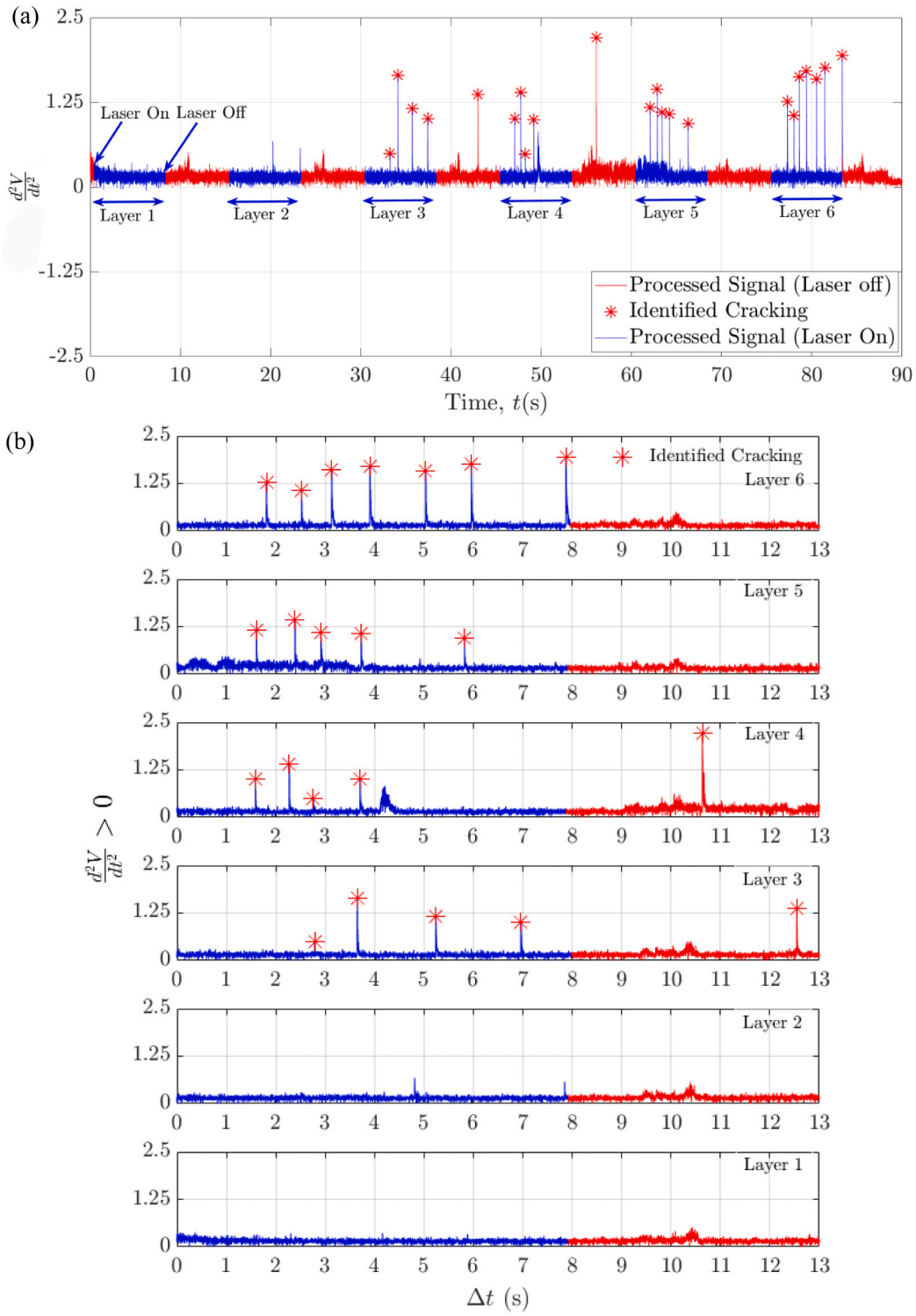

Fig. 5. Analysis of processed signals generated during the DED process under low energy density conditions. (a) Comprehensive results showing identified crack events across all layers (b) layer-by-layer breakdown of crack events distribution.

potential delayed crack occurrences resulting from residual stress accumulation in the manufactured structures. Layer-by-layer analysis was conducted to identify cracks and assess whether the reformation of cracks occurred when the laser beam scanned over pre-existing cracks. Additionally, it was investigated whether residual stress accumulation in the manufactured structures contributed to delayed crack occurrences in different layers. This comprehensive approach enabled a detailed examination of crack initiation and propagation, offering crucial information about the relationship between process parameters, residual stress, and crack formation across multiple layers. The layer-by-layer analysis of crack formation in the deposited track reveals a complex evolution of residual stress buildup and its impact on crack initiation and propagation. Initially, Layer 1 and 2 showed no detectable cracks, suggesting a relatively stable deposition. However, crack initiation began in Layer 3, with four cracks detected at 2.7 s, 3.6 s, 5.2 s, and 6.9 s during deposition and one delayed crack occurred after 4.6 s after the

laser scanning finished. This indicated that by Layer 3, residual stresses and thermal gradients had accumulated sufficiently to overcome the material's crack resistance. The crack formation pattern continued in subsequent layers, with pre-existing cracks undergoing remelting during the deposition of new material. As residual stresses accumulated, new cracks formed in the freshly deposited layers, often extending through the locations of previous cracks. This process resulted in a continuous network of cracks propagating through multiple layers of the deposited material.

Consequently, four cracks were identified at 1.5 s, 2.2 s, 2.7 s, and 3.7 s, with an additional crack occurring at 10.6 s, approximately 2.5 s following the completion of Layer 4. The occurrence of delayed cracks (e.g., 4.6 s after laser scanning in the Layer 3, 2.5 s after deposition in the Layer 4 indicates the continued evolution of residual stresses even after deposition, likely due to cooling and solidification processes. The growth of the first four existing cracks continued into Layer 5, with slightly delayed occurrence times of 1.6 s, 2.3 s, 2.9 s, and 3.7 s, respectively, and another crack occurring at 5.8 s. A significant increase in crack formation was observed in Layer 6, with seven cracks detected at 1.8 s, 2.5 s, 3.1 s, 3.9 s, 5.0 s, 5.9 s, and 7.8 s, respectively. This observed delay in crack formation from Layer 4 to Layer 6 can be primarily due to the evolving cooling rate among the deposited layers. While the DED process typically exhibits high cooling rates ranging from 102 to 104 K/s, resulting in rapid solidification, [53,54] as the layer number increases, heat accumulation becomes more pronounced owing to decreased temperature gradients and limited heat dissipation. This thermal buildup leads to an expansion of the melt pool size and a consequent reduction in the cooling rate [55]. These thermal effects collectively contribute to the delayed onset of crack formation in higher layers, highlighting the critical role of cooling rate in the crack formation mechanism during the DED process.

The DED process, characterized by layer-by-layer material addition, subjects the fabricated component to multiple thermal cycles. As each layer is deposited, it undergoes rapid heating and subsequent cooling, leading to thermal expansion and contraction. This cyclical thermal behaviour progressively contributes to the accumulation of residual stresses within the material. The observed increase in crack formation from Layer 5 to Layer 6, as evidenced by the higher number of detected cracks, suggests that the accumulated residual stresses create conditions favourable to both the propagation of existing cracks and the initiation of new ones as more layers are deposited.

To confirm the accuracy of the acoustic analysis, the fabricated track underwent longitudinal sectioning for physical examination. This examination revealed a close correspondence between the number of cracks physically observed and those detected by the AE analysis in the Layer 6, see Fig. 6. This alignment between the acoustic analysis and the physical inspection confirms the accuracy of the AE-based crack detection technique. The consistency in the number of identified cracks across both methods underscores the reliability of the AE analysis in detecting and characterizing crack events during the DED process.

The analysis of the sample deposited under high energy density conditions, revealed a distinct pattern of crack formation across its six layers. As presented in Fig. 7, the analysis timeframe spans from $t = 0$ s, representing the start of deposition, to $t = 13$ s, extending beyond the completion of the deposition process at $t = 9$ s. The analysis timeframe beyond the deposition completion (from 9 s to 13 s) allows for the observation of delayed crack occurrences. Layer 1 exhibited the highest number of cracks, with a total of 17 identified. The early onset of cracking (starting from Layer 1, compared to the low energy density parameters) and the high number of cracks in Layer 1 indicate that high energy density parameters may lead to increased thermal gradients and residual stress, promoting crack formation from the initial stages of deposition.

The longitudinal sectioning of the sample revealed a total of 16 cracks (Fig. 8), while the AE analysis detected varying numbers of cracks per layer: 17 in Layer 1, 15 in Layer 2, 16 in Layer 3, and 15 each in layers 4, 5, and 6. Notably, the AE analysis detected 17 cracks in Layer 1, one more than the physical examination. The overestimation in Layer 1 can be attributed to one crack generating multiple acoustic events due to the large number of cracks generate in a short period of time. This phenomenon was observed by Ito et al. [56] who indicated that one microcracks might generate multiple acoustic events. The AE analysis showed consistent results with the physical examination for Layer 3 through identifying 16 cracks. However, for layers 2, 4, 5, and 6, the AE analysis detected 15 cracks per layer, failing to identify one crack in each of these layers compared to the longitudinal sectioning results.

The slight underestimation in crack count for Layers 2, 4, 5, and 6 might be attributed to several factors. Partial healing of cracks during remelting could contribute to this discrepancy. Additionally, the acoustic properties of crack events and the industrial environment play a role. In a noisy industrial setting, the lower acoustic power of crack events makes them more susceptible to being masked or attenuated by ambient noise and external disturbances. The STFT analysis revealed that crack events and disturbances exhibit prominence in overlapping

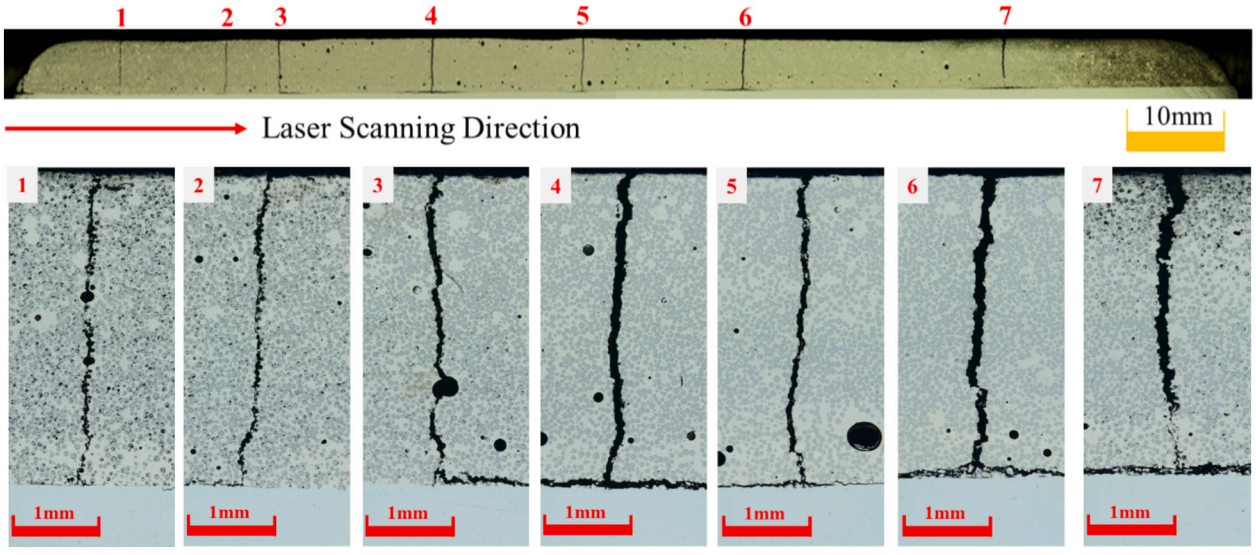

Fig. 6. Microscope imaging of the longitudinal section of the single track deposited under low energy density conditions. Top: Full view of the sectioned track illustrating the laser scanning direction from left to right. Bottom: Magnified micrographs highlighting interlayer cracks observed within the deposited layers.

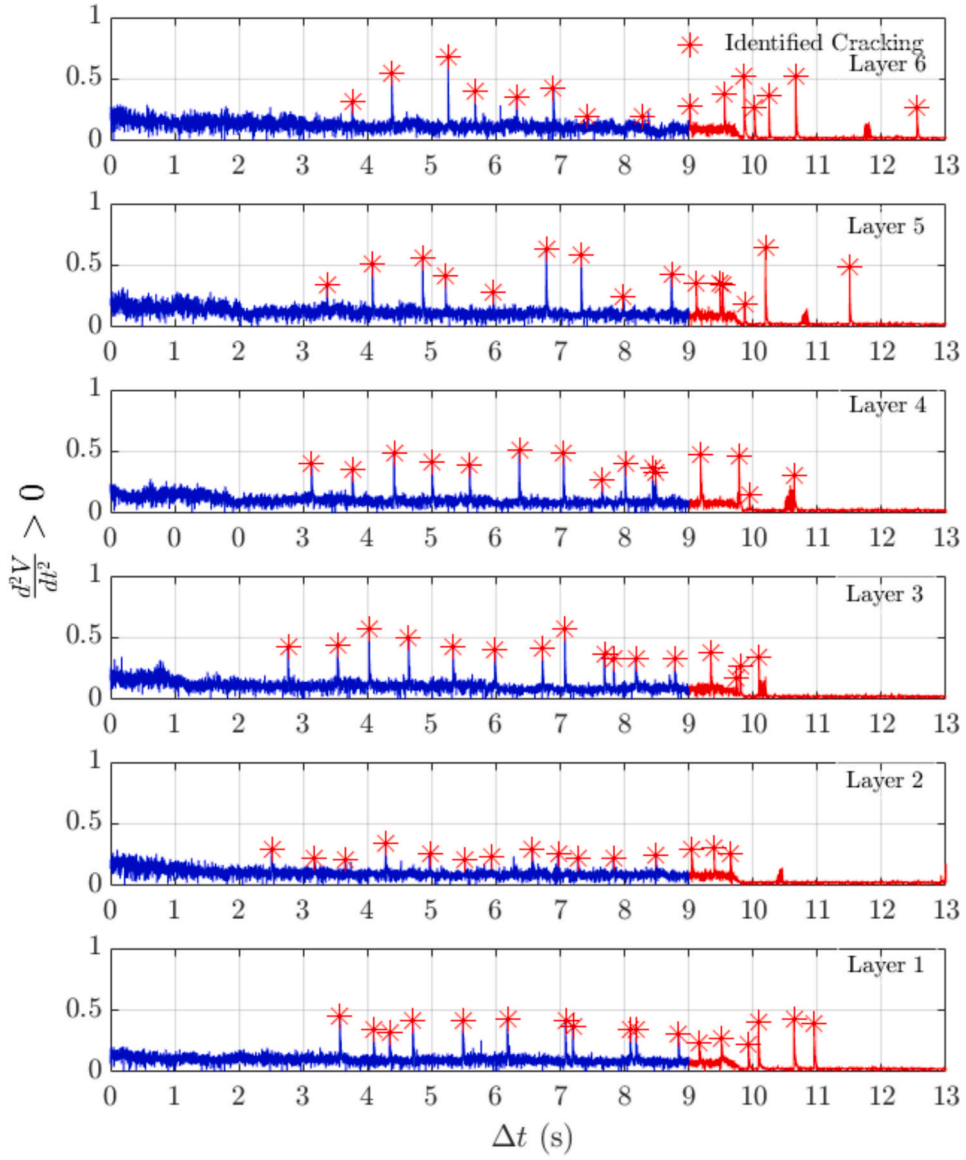

Fig. 7. Layer-by-layer analysis of the processed acoustic signals generated during the fabrication of Track 2.

frequency ranges (4–18 kHz for cracks, 8–18 kHz for disturbances) in our workshop environments. This overlap, in some cases poses challenges in distinguishing crack signals from disturbances.

The analysis of crack formation patterns in the sample deposited using high energy density process parameters reveals a complex interplay between thermal gradients and residual stress accumulation across multiple layers. In this track, crack formation begins in Layer 1, with the first crack generating at 3.5 s. A significant number of cracks are generated throughout the deposition process, and the formation of cracks continues even after the deposition process was completed. As Layer 1 was deposited onto the substrate, the thermal expansion mismatch between the deposited material and the substrate contributed to the initial residual stress accumulation. This developed residual stress acted as a driving force for crack initiation. Similar phenomena were observed in subsequent layers, with pre-existing cracks being remelted, newly deposited material cracking again, generating acoustic events, and the newly formed cracks propagating through the previous cracks [57,58]. Layer 2 exhibited early reformation of pre-existing cracks, with the first crack detected at 2.5 s. However, a progressive delay in crack formation was observed from Layer 3 to Layer 6, with the first crack initiation occurring at 2.7 s, 3.1 s, 3.3 s, and 3.7 s, respectively. This delay can be attributed to the high energy density parameters used in the DED process, which result in larger melt pools. Due to the inverse relationship between cooling rate and energy density [54], these melt pools remained in a liquid state for an extended period, thereby delaying solidification. This extended liquid state results in a slower overall cooling rate for the deposited material. The prolonged liquid state allows more time for thermal stresses to develop gradually within the material as it cools. As a result of the slower cooling and gradual stress accumulation, the material requires more time to build up sufficient stress to initiate cracking in these later layers.

The investigation revealed distinct crack formation patterns in samples deposited using low and high energy density parameters during the DED process. In the low energy density sample, crack initiation was delayed, occurring only after several layers were deposited. This suggests that thermal stresses and residual strains gradually accumulated across multiple layers before reaching a critical level for crack formation. A progressive delay in crack initiation was observed in subsequent layers, suggesting a gradual buildup of residual stress.

In contrast, the high energy density parameters led to increased thermal gradients and residual stress, resulting in crack generation from the Layer 1. Notably, numerous cracks occurred post-laser deposition,

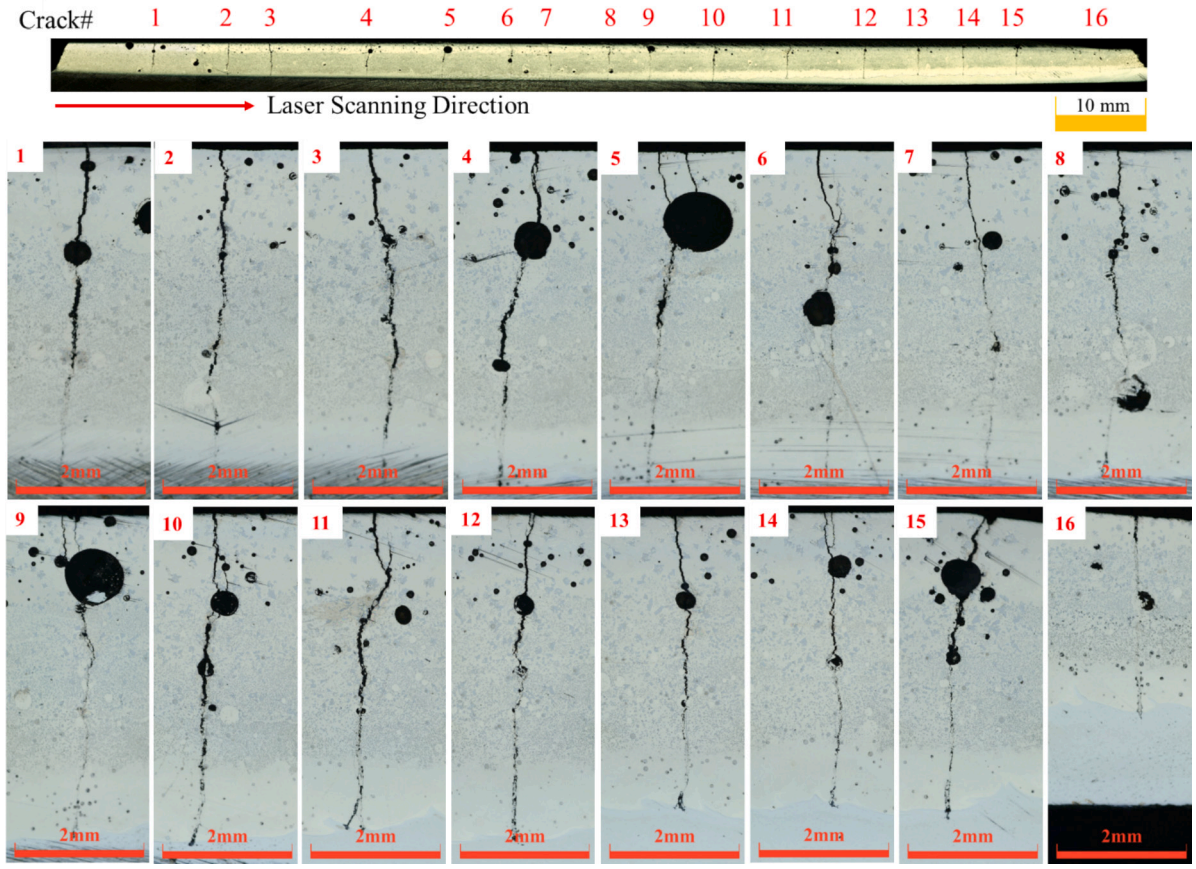

Fig. 8. Microscope imaging of the longitudinal section of the single track deposited under high energy density conditions. Top: Full view of the sectioned track illustrating the laser scanning direction from left to right. Bottom: Magnified micrographs highlighting interlayer cracks observed within the deposited layers.

suggesting continued stress evolution even after deposition. The sample deposited utilizing high energy density conditions also demonstrated an increasingly pronounced progressive delay in crack initiation compared to the low energy density sample, suggesting a more complex stress state in higher energy density conditions. These findings support the hypothesis that energy density critically influences thermal gradient and residual stress generation in the deposited part.

The longitudinal sectioning of the sample deposited using high energy density parameters revealed a total of 16 physical cracks, as illustrated in Fig. 8 while the AE analysis detected 15 cracks in Layer 6. Although the AE-based crack detection system underestimated the crack count by one, the overall performance across the experiments was robust. Across the two fabricated multi-layer single tracks, the AE method successfully identified 22 out of 23 physical cracks. The strong correlation between the acoustic emission analysis and physical crack examination highlights the reliability and effectiveness of the developed AE-based crack detection system for monitoring the DED process, demonstrating its potential as a robust tool for real-time quality control

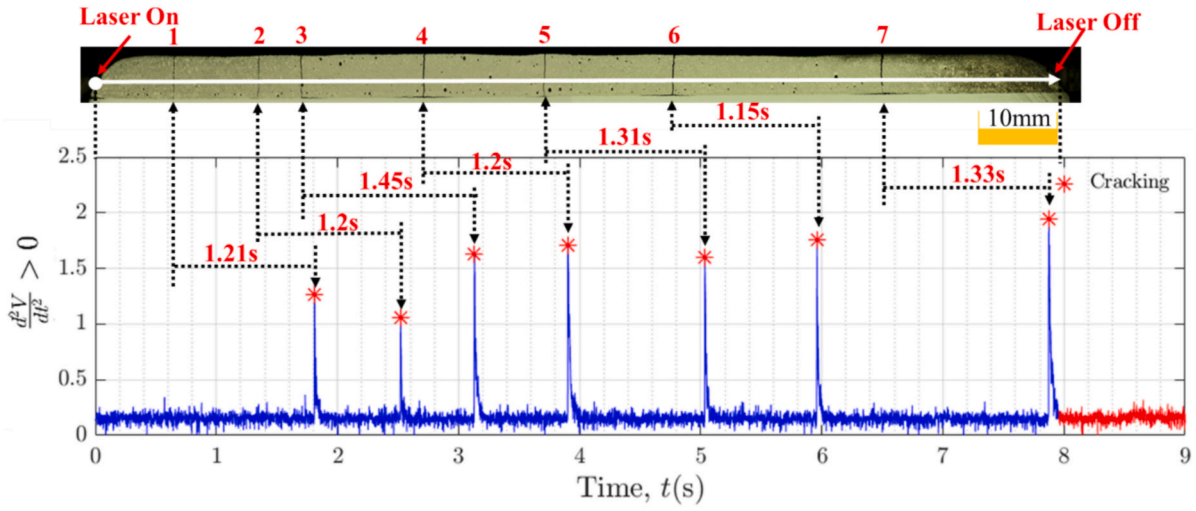

Fig. 9. Time delay between laser beam passage and acoustic emission-based crack detection in Layer 6 of Track 1.

in AM process.

4.2. Crack locations relative to the laser beam

The layer-by-layer acoustic signal analysis revealed a complex temporal relationship between laser-material interaction and crack formation in the DED process. To quantify the temporal relationship, the physical locations of individual cracks were correlated with their corresponding acoustic signals in Layer 6 of the samples deposited using low and high energy density parameters (Fig. 9 and Fig. 10, respectively). In the case of the low energy density sample, acoustic analysis detected seven cracks at 1.8 s, 2.5 s, 3.1 s, 3.9 s, 5.0 s, 5.9 s, and 7.8 s, respectively. The calculated crack positions based on acoustic data (using crack occurrence times and laser scanning speed) were compared with the actual measured physical locations of cracks. The comparison revealed a consistent time lag between the laser beam's passage and the detection of cracks. This delay, ranging from 1.15 to 1.33 s, is unlikely to be attributed to systematic errors or equipment limitations. Instead, it likely represents the time necessary for residual stresses to accumulate and reach a critical threshold, at which point the crack becomes sufficiently pronounced to emit detectable acoustic signals. This observation suggests that crack formation and propagation occur during the cooling and solidification phases, rather than immediately upon laser irradiation.

A similar methodology was employed to calculate the delay in the sample deposited using high energy density parameters, revealing an observed delay range of 2.71 s to 3.92 s, which is significantly higher than the 1.15 s to 1.33 s range observed in the low energy density sample. This increased delay can be attributed to the higher energy input used in the deposition process for the high energy density sample. The higher energy input likely results in several interrelated effects. Firstly, it may produce a larger melt pool that retains its liquid phase for an extended period, thereby delaying the onset of solidification and subsequent crack formation. Secondly, the increased energy density generates steeper temperature gradients within the material, leading to a slower rate of solidification and more intricate thermal distributions. These pronounced thermal gradients can significantly influence stress distribution and solidification dynamics. Furthermore, the higher energy input can induce greater thermal expansion and contraction during the deposition process, resulting in elevated residual stresses within the fabricated structures. Consequently, these increased stresses may require more time to reach the critical level necessary for crack initiation and propagation, thus contributing to the extended delay observed in the high energy density sample. These results, which closely align with the findings of Tristan et al. [37] who observed crack growth approximately 500 ms after the laser beam traversed pre-existing cracks using synchrotron X-ray imaging techniques, further validate the effectiveness of our AE-based method in detecting and analysing crack formation dynamics in the DED process.

Utilizing the observed time delay and laser scanning speed, we calculated the spatial relationship between crack formation and laser beam position. Our findings reveal that cracks were generated approximately 19–22 mm behind the laser beam for the low energy density sample and 36–53 mm for the high energy density sample. These distances were normalized using the laser spot diameter (4.8 mm) to provide a more standardized comparison, as illustrated in Fig. 11.

For the low energy density sample, cracks were generated approximately 3.9 to 4.6 times the beam's spot size behind the laser beam's current position, while for the high energy density sample, this distance increased to 7.5 to 11 times the beam's spot size, as presented in Fig. 11. This significant distance indicates that crack formation occurs during the solidification and cooling phases of the deposited layer, well behind the melt pool. Thermal information derived solely from the melt pool is insufficient for completely characterizing the dynamics of crack initiation, growth, and propagation during the DED process. To comprehensively understand these phenomena, it is crucial to examine the region trailing the melt pool, focusing on complex thermal gradients, residual stress development, and solidification dynamics that contribute to crack formation. This observation underscores the importance of considering the entire thermal history of the deposited material, including cooling rates and thermal cycling, to accurately predict and mitigate crack formation in DED process.

5. Conclusion

This study employed an AE based process monitoring method for detecting and locating both surface and subsurface cracks in the DED process. The layer-by-layer analysis of acoustic signals revealed that crack formation occurs both during the deposition process and after laser deactivation, indicating the complex nature of residual stress development and relief in DED-manufactured structures. A significant time lag between laser-material interaction and crack formation was

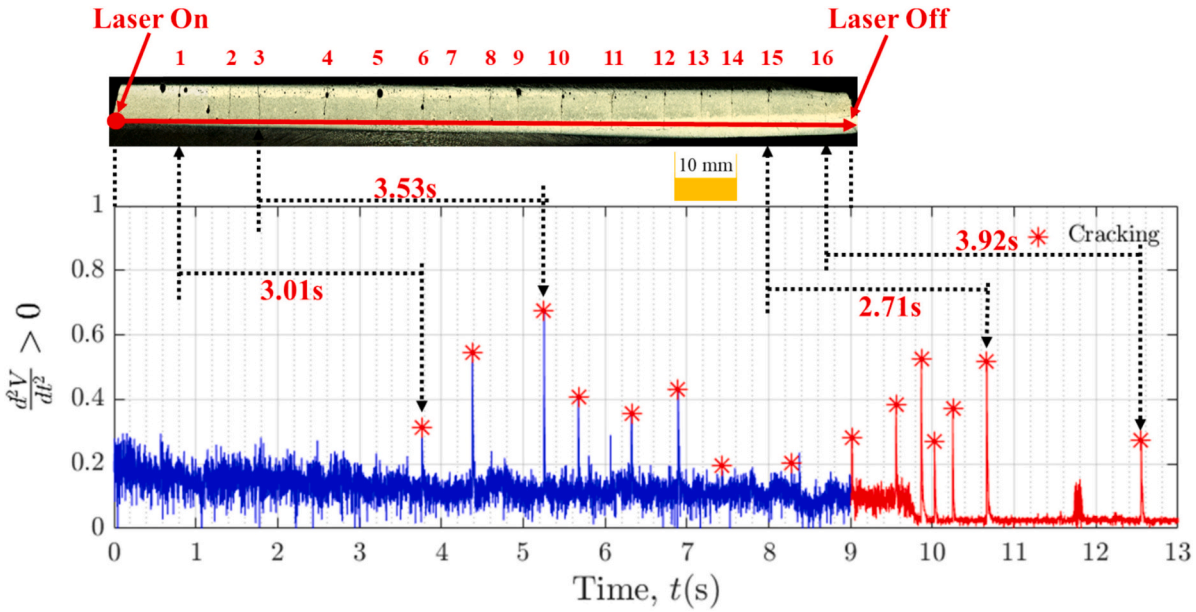

Fig. 10. Time delay between laser beam passage and acoustic emission-based crack detection in Layer 6 of Track 2.

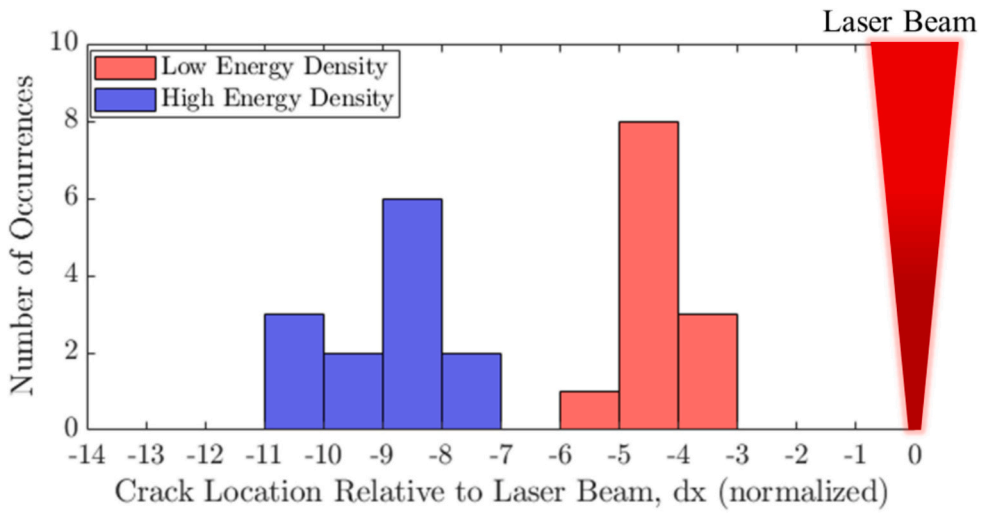

Fig. 11. Spatial distribution of crack formation relative to laser beam position in DED process.

observed, attributed to the applied energy density. The magnitude of this delay was directly influenced by the energy input, with higher energy densities resulting in more pronounced delays.

The key findings and novelty of this research are:

- The employed AE-based monitoring system demonstrated high precision in detecting and locating both surface and subsurface cracks in the DED process, showing excellent agreement with physical crack examination.
- The layer-by-layer analysis of acoustic signals provided crucial information on crack distribution and formation dynamics, facilitating real-time process adjustments to mitigate crack formation and improve product quality in DED manufacturing.
- A quantitative relationship was established between energy input and the delay in crack initiation and propagation during the DED process. Under low energy density conditions, acoustic emissions indicative of crack formation was detected 1.15 to 1.33 s after the laser beam traversed the crack initiation zone, whereas high energy density conditions resulted in significantly longer detection delays of 2.71 to 3.92 s. This delay is attributed to extended melt pool lifetime, slower cooling rates, and complex thermal gradients under high-energy conditions, which influence residual stress buildup and alter crack formation dynamics.
- The study revealed specific data on crack formation location relative to the laser beam position. For low energy density, cracks were generated approximately 3.9 to 4.6 times the beam's spot size behind the laser beam's current position, while for high energy density, this distance increased to 7.5 to 11 times the beam's spot size. The substantial distance between crack formation and the laser beam position indicates that crack formation occurs during solidification and cooling phases, well behind the melt pool.

This study provided valuable insights into the layer-by-layer formation of cracks during the DED process. By identifying the specific locations and timings of cracks, manufacturers gained the capability to understand when and where defects occur in manufactured components. This enables manufacturers to adjust their processes as necessary, potentially eliminating the need for post-process quality inspections. While previous research has explored the temporal and spatial dynamics of crack propagation between deposited layers using X-ray imaging techniques, this study represents the first application of an inexpensive AE technique to provide such insights. The results significantly enhance our understanding of the complex mechanisms underlying crack formation and propagation, offering crucial information that can inform mitigation strategies aimed at improving process reliability and overall part quality.

Future work will focus on the implementation of wavelet-based acoustic beamforming utilizing a 48-channel microphone array to enhance the localization accuracy of crack events during the DED process. This technique, commonly employed in the aerospace industry for identifying short-duration acoustic sources, is anticipated to significantly improve the spatial resolution and reliability of crack detection. Subsequent efforts will aim to integrate this system into industrial DED environments for real-time monitoring and adaptive process control.

CRediT authorship contribution statement

Md Jonaet Ansari: Writing – original draft, Validation, Methodology, Investigation, Conceptualization. **Anthony Roccisano:** Writing – review & editing, Supervision, Conceptualization. **Elias J.G. Arcondoulis:** Writing – review & editing, Supervision, Conceptualization. **Christiane Schulz:** Writing – review & editing, Supervision. **Thomas Schläfer:** Writing – review & editing, Supervision. **Colin Hall:** Writing – review & editing, Supervision, Conceptualization.

Declaration of competing interest

The authors declare that they have no known competing financial interests or personal relationships that could have appeared to influence the work reported in this paper.

Acknowledgments

The authors acknowledge the support from the Australian Research Council (ARC). The ARC Training Centre in Surface Engineering for Advanced Materials, SEAM, has been funded under the ARC Industrial Transformation Training Centre (ITTC) scheme via Award IC180100005. We are grateful for the additional support of the industrial, university and other organisation partners who have contributed to the establishment and support of SEAM.

The authors acknowledge the instruments and expertise of Microscopy Australia at the Future Industries Institute, University of South Australia, enabled by NCRIS, university, and state government support. This work used the NCRIS and Government of South Australia enabled Australian National Fabrication Facility - South Australian Node (ANFF-SA).

References

[1] Hatem A, Schulz C, Schlaefer T, Boobhun JT, Stanford N, Hall C. Influence of laser absorption by water- and gas-atomised powder feedstock on laser metal deposition of AISI 431 stainless steel. Addit Manuf 2021;47:102242. https://doi.org/10.1016/j.addma.2021.102242.

[2] Da Silva A, Frostevarg J, Kaplan AFH. Melt pool monitoring and process optimisation of directed energy deposition via coaxial thermal imaging. J Manuf Process 2023;107:126–33. https://doi.org/10.1016/j.jmapro.2023.10.021.

[3] Khanzadeh M, Chowdhury S, Marufuzzaman M, Tschopp MA, Bian L. Porosity prediction: supervised-learning of thermal history for direct laser deposition. J Manuf Syst 2018;47:69–82. https://doi.org/10.1016/j.jmsy.2018.04.001.

[4] Kim S, Kim E-H, Lee W, Sim M, Kim I, Noh J, et al. Real-time in-process control methods of process parameters for additive manufacturing. J Manuf Syst 2024;74:1067–90. https://doi.org/10.1016/j.jmsy.2024.05.008.

[5] Cai Y, Xiong J, Chen H, Zhang G. A review of in-situ monitoring and process control system in metal-based laser additive manufacturing. J Manuf Syst 2023;70:309–26. https://doi.org/10.1016/j.jmsy.2023.07.018.

[6] Grandhi M, Nguyen V, Liu Z, Romo-De-La-cruz C-O, Song X. Copper-nickel functionally magnetic gradient material fabricated via directed energy deposition. J Manuf Process 2023;100:47–54. https://doi.org/10.1016/j.jmapro.2023.05.014.

[7] Akhavan J, Lyu J, Mahmoud Y, Xu K, Vallabh CKP, Manoochehri S. Dataset of in-situ coaxial monitoring and print's cross-section images by direct energy deposition fabrication. Sci Data 2023;10:776. https://doi.org/10.1038/s41597-023-02672-4.

[8] Leroy-Dubief C, Poulhaon F, Joyot P. Regulation strategy for directed energy deposition-laser powder process based on working distance modulation: modelling and application to thin wall configurations. J Manuf Process 2023;104:307–21. https://doi.org/10.1016/j.jmapro.2023.09.008.

[9] Shi S, Liu X, Wang Z, Chang H, Wu Y, Yang R, et al. An intelligent process parameters optimization approach for directed energy deposition of nickel-based alloys using deep reinforcement learning. J Manuf Process 2024;120:1130–40. https://doi.org/10.1016/j.jmapro.2024.05.001.

[10] Brennan M, Keist JS, Palmer TA. Defects in Metal Additive Manufacturing Processes. In: Bourell DL, Frazier W, Kuhn H, Seifi M, editors. Additive manufacturing processes. ASM International; 2020. p. 277–86. https://doi.org/10.31399/asm.hb.v24.a0006557.

[11] Zhang Y, Guo B, Li J, Wang Z, Wang J. Predicting solidification cracking in directed energy deposition of Hastelloy X alloys based on thermal-mechanical model. J Manuf Process 2023;101:561–75. https://doi.org/10.1016/j.jmapro.2023.06.033.

[12] Lee S, Kim J, Shim D-S, Park S-H, Choi YS. Micro-cracking in medium-carbon steel layers additively deposited on gray cast Iron using directed energy deposition. Met Mater Int 2020;26:708–18. https://doi.org/10.1007/s12540-019-00589-5.

[13] Chen Y, Lu F, Zhang K, Nie P, Elmi Hosseini SR, Feng K, et al. Dendritic microstructure and hot cracking of laser additive manufactured Inconel 718 under improved base cooling. J Alloys Compd 2016;670:312–21. https://doi.org/10.1016/j.jallcom.2016.01.250.

[14] Park G-W, Shin S, Kim J-Y, Koo Y-M, Lee W, Lee K-A, et al. Analysis of solidification microstructure and cracking mechanism of a matrix high-speed steel deposited using directed-energy deposition. J Alloys Compd 2022;907:164523. https://doi.org/10.1016/j.jallcom.2022.164523.

[15] Li Y, Chen K, Tamura N. Mechanism of heat affected zone cracking in Ni-based superalloy DZ125L fabricated by laser 3D printing technique. Mater Des 2018;150:171–81. https://doi.org/10.1016/j.matdes.2018.04.032.

[16] Zimermann R, Mohseni E, Foster EA, Vasilev M, Loukas C, Vithanage RKW, et al. In-process non-destructive evaluation of metal additive manufactured components at build using ultrasound and eddy-current approaches. J Manuf Process 2023;107:549–58. https://doi.org/10.1016/j.jmapro.2023.10.063.

[17] Chua C, Liu Y, Williams RJ, Chua CK, Sing SL. In-process and post-process strategies for part quality assessment in metal powder bed fusion: a review. J Manuf Syst 2024;73:75–105. https://doi.org/10.1016/j.jmsy.2024.01.004.

[18] Haley J, Karandikar J, Herberger C, MacDonald E, Feldhausen T, Lee Y. Review of in situ process monitoring for metal hybrid directed energy deposition. J Manuf Process 2024;109:128–39. https://doi.org/10.1016/j.jmapro.2023.12.004.

[19] Taherkhani K, Ero O, Liravi F, Toorandaz S, Toyserkani E. On the application of in-situ monitoring systems and machine learning algorithms for developing quality assurance platforms in laser powder bed fusion: a review. J Manuf Process 2023;99:848–97. https://doi.org/10.1016/j.jmapro.2023.05.048.

[20] Era IZ, Farahani MA, Wuest T, Liu Z. Machine learning in directed energy deposition (DED) additive manufacturing: a state-of-the-art review. Manuf Lett 2023;35:689–700. https://doi.org/10.1016/j.mfglet.2023.08.079.

[21] Sahar T, Rauf M, Murtaza A, Khan LA, Ayub H, Jameel SM, et al. Anomaly detection in laser powder bed fusion using machine learning: a review. Results Eng 2023;17:100803. https://doi.org/10.1016/j.rineng.2022.100803.

[22] Li B, Zhang Y, Lei Y, Wei H, Chen C, Liu F, et al. A single-sensor multi-scale quality monitoring methodology for laser-directed energy deposition: example with height instability and porosity monitoring in additive manufacturing of ceramic thin-walled parts. Addit Manuf 2024;79:103923. https://doi.org/10.1016/j.addma.2023.103923.

[23] Guerra MG, Mazzarisi M, Latte M, Lavecchia F, Campanelli S, Galantucci LM. Off-axis monitoring of the melt pool spatial information in laser metal deposition process. Proc CIRP 2024;121:144–9. https://doi.org/10.1016/j.procir.2023.08.063.

[24] Yin M, Zhuo S, Xie L, Chen L, Wang M, Liu G. Online monitoring of local defects in robotic laser additive manufacturing process based on a dynamic mapping strategy and multibranch fusion convolutional neural network. J Manuf Syst 2023;71:494–503. https://doi.org/10.1016/j.jmsy.2023.10.005.

[25] Wang K. Contrastive learning-based semantic segmentation for in-situ stratified defect detection in additive manufacturing. J Manuf Syst 2023;68:465–76. https://doi.org/10.1016/j.jmsy.2023.05.001.

[26] Kim J, Yang Z, Ko H, Cho H, Lu Y. Deep learning-based data registration of melt-pool-monitoring images for laser powder bed fusion additive manufacturing. J Manuf Syst 2023;68:117–29. https://doi.org/10.1016/j.jmsy.2023.03.006.

[27] Jafari-Marandi R, Khanzadeh M, Tian W, Smith B, Bian L. From in-situ monitoring toward high-throughput process control: cost-driven decision-making framework for laser-based additive manufacturing. J Manuf Syst 2019;51:29–41. https://doi.org/10.1016/j.jmsy.2019.02.005.

[28] Oster S, Breese PP, Ulbricht A, Mohr G, Altenburg SJ. A deep learning framework for defect prediction based on thermographic in-situ monitoring in laser powder bed fusion. J Intell Manuf 2023;35(4):1687–706. https://doi.org/10.1007/s10845-023-02117-0.

[29] D'Accardi E, Chiappini F, Giannasi A, Guerrini M, Maggiani G, Palumbo D, et al. Online monitoring of direct laser metal deposition process by means of infrared thermography. Prog Addit Manuf 2023;9(4):983–1001. https://doi.org/10.1007/s40964-023-00496-7.

[30] Altenburg SJ, Straße A, Gumenyuk A, Maierhofer C. In-situ monitoring of a laser metal deposition (LMD) process: comparison of MWIR, SWIR and high-speed NIR thermography. Quant InfraRed Thermogr J 2020;19(2):1–18. https://doi.org/10.1080/17686733.2020.1829889.

[31] Dong W, Lian J, Yan C, Zhong Y, Karnati S, Guo Q, et al. Deep-learning-based segmentation of keyhole in in-situ X-ray imaging of laser powder bed fusion. Materials 2024;17:510. https://doi.org/10.3390/ma17020510.

[32] Vaghefi E. Volumetric defect classification in nano-resolution X-ray computed tomography images of laser powder bed fusion via deep learning. J Manuf Process 2024;121:499–511. https://doi.org/10.1016/j.jmapro.2024.05.030.

[33] Bimrose MV, Hu T, McGregor DJ, Wang J, Tawfick S, Shao C, et al. Detecting and classifying hidden defects in additively manufactured parts using deep learning and X-ray computed tomography. J Intell Manuf 2024. https://doi.org/10.1007/s10845-024-02416-0.

[34] Wolff SJ, Wu H, Parab N, Zhao C, Ehmann KF, Sun T, et al. In-situ high-speed X-ray imaging of piezo-driven directed energy deposition additive manufacturing. Sci Rep 2019;9:962. https://doi.org/10.1038/s41598-018-36678-5.

[35] Chen Y, Zhang D, O'Toole P, Qiu D, Seibold M, Schricker Klaus, et al. In situ observation and reduction of hot-cracks in laser additive manufacturing. Commun Mater 2024;5:84. https://doi.org/10.1038/s43246-024-00522-3.

[36] Ghasemi-Tabasi H, De Formanoir C, Van Petegem S, Jhabvala J, Hocine S, Boillat E, et al. Direct observation of crack formation mechanisms with operando laser powder bed fusion X-ray imaging. Addit Manuf 2022;51:102619. https://doi.org/10.1016/j.addma.2022.102619.

[37] Fleming TG, Rees DT, Marussi S, Connolley T, Atwood RC, Jones MA, et al. In situ correlative observation of humping-induced cracking in directed energy deposition of nickel-based superalloys. Addit Manuf 2023;71:103579. https://doi.org/10.1016/j.addma.2023.103579.

[38] AbouelNour Y, Gupta N. In-situ monitoring of sub-surface and internal defects in additive manufacturing: a review. Mater Des 2022;222:111063. https://doi.org/10.1016/j.matdes.2022.111063.

[39] Kononenko DY, Nikonova V, Seleznev M, Van Den Brink J, Chernyavsky D. An in situ crack detection approach in additive manufacturing based on acoustic emission and machine learning. Addit Manuf Lett 2023;5:100130. https://doi.org/10.1016/j.addlet.2023.100130.

[40] Taheri H, Koester LW, Bigelow TA, Faierson EJ, Bond LJ. In situ additive manufacturing process monitoring with an acoustic technique: clustering performance evaluation using K-means algorithm. J Manuf Sci Eng 2019;141:041011. https://doi.org/10.1115/1.4042786.

[41] Li K, Li T, Ma M, Wang D, Deng W, Lu H. Laser cladding state recognition and crack defect diagnosis by acoustic emission signal and neural network. Opt Laser Technol 2021;142:107161. https://doi.org/10.1016/j.optlastec.2021.107161.

[42] García de la Yedra A, Pfleger M, Aramendi B, Cabeza M, Zubiri F, Mitter T, et al. Online cracking detection by means of optical techniques in laser-cladding process. Struct Control Health Monit 2019;26:e2291. https://doi.org/10.1002/stc.2291.

[43] Kim H-S, Park S-H. Acoustic signal monitoring using audible cracking sounds for efficient in-situ crack detection in laser directed energy deposition of hard surfaces. Addit Manuf Lett 2024;9:100210. https://doi.org/10.1016/j.addlet.2024.100210.

[44] Song JY, Dass A, Moridi A, McLaskey GC. Detection of defects during laser-powder interaction by acoustic emission sensors and signal characteristics. Addit Manuf 2024;82:104035. https://doi.org/10.1016/j.addma.2024.104035.

[45] Wang H, Zhang S, Li B. Machine learning-assisted acoustic emission monitoring for track formability prediction of laser powder bed fusion. Mater Today Commun 2024;38:108522. https://doi.org/10.1016/j.mtcomm.2024.108522.

[46] Pandiyan V, Wróbel R, Richter RA, Leparoux M, Leinenbach C, Shevchik S. Monitoring of laser powder bed fusion process by bridging dissimilar process maps using deep learning-based domain adaptation on acoustic emissions. Addit Manuf 2024;80:103974. https://doi.org/10.1016/j.addma.2024.103974.

[47] Pandiyan V, Wróbel R, Leinenbach C, Shevchik S. Optimizing in-situ monitoring for laser powder bed fusion process: deciphering acoustic emission and sensor sensitivity with explainable machine learning. J Mater Process Technol 2023;321:118144. https://doi.org/10.1016/j.jmatprotec.2023.118144.

[48] Li S, Chen B, Tan C, Song X. In situ identification of laser directed energy deposition condition based on acoustic emission. Opt Laser Technol 2024;169:110152. https://doi.org/10.1016/j.optlastec.2023.110152.

[49] Chen L, Yao X, Moon SK. In-situ acoustic monitoring of direct energy deposition process with deep learning-assisted signal denoising. Mater Today Proc 2022;70:136–42. https://doi.org/10.1016/j.matpr.2022.09.008.
[50] Chen L, Yao X, Tan C, He W, Su J, Weng F, et al. In-situ crack and keyhole pore detection in laser directed energy deposition through acoustic signal and deep learning. Addit Manuf 2023;69:103547. https://doi.org/10.1016/j.addma.2023.103547.
[51] Chen L, Bi G, Yao X, Tan C, Su J, Ng NPH, et al. Multisensor fusion-based digital twin for localized quality prediction in robotic laser-directed energy deposition. Robot Comput Integr Manuf 2023;84:102581. https://doi.org/10.1016/j.rcim.2023.102581.
[52] Ansari MJ, Arcondoulis EJG, Roccisano A, Schulz C, Schlaefer T, Hall C. Optimized analytical approach for the detection of process-induced defects using acoustic emission during directed energy deposition process. Addit Manuf 2024;86:104218. https://doi.org/10.1016/j.addma.2024.104218.
[53] Büßenschütt K, Köhnen P, Kies F, Koß S, Schleifenbaum JH, Haase C. High-speed direct energy deposition as a high-throughput design tool for laser-based additive manufacturing. Addit Manuf Lett 2024;8:100188. https://doi.org/10.1016/j.addlet.2023.100188.
[54] Jeong J, Webster S, Liao S, Mogonye J-E, Ehmann K, Cao J. Cooling rate measurement in directed energy deposition using photodiode-based planck thermometry (PDPT). Addit Manuf Lett 2022;3:100101. https://doi.org/10.1016/j.addlet.2022.100101.
[55] Nair AM, Muvvala G, Sarkar S, Nath AK. Real-time detection of cooling rate using pyrometers in tandem in laser material processing and directed energy deposition. Mater Lett 2020;277:128330. https://doi.org/10.1016/j.matlet.2020.128330.
[56] Ito K, Kusano M, Demura M, Watanabe M. Detection and location of microdefects during selective laser melting by wireless acoustic emission measurement. Addit Manuf 2021;40:101915. https://doi.org/10.1016/j.addma.2021.101915.
[57] Wang S, Yu C, Yin H, Li C, Wang H, Miao Y, et al. The mechanism and regulation of hot cracking in a new complex-concentrated alloy by a novel integrated directed energy deposition. Addit Manuf 2024;80:103948. https://doi.org/10.1016/j.addma.2023.103948.
[58] Mo B, Li T, Shi F, Deng L, Liu W. Crack initiation and propagation within nickel-based high-temperature alloys during laser-based directed energy deposition: a review. Opt Laser Technol 2024;179:111327. https://doi.org/10.1016/j.optlastec.2024.111327.